Spatial Desynchronization of Glycolytic Waves as Revealed by Karhunen−Loève Analysis†

Satenik Bagyan,‡ Thomas Mair,‡ Yuri Suchorski,§ Marcus J. B. Hauser,‡ and Ronny Straube*,⊥

Biophysics Group, Institute of Experimental Physics, Otto-von-Guericke University, Universitätsplatz 2, 39106 Magdeburg, Germany, Institute of Materials Chemistry, Vienna University of Technology, Veterinärplatz 1, A-1210 Vienna, Austria, and Department of Systems Biology, Max-Planck-Institute for Dynamics of Complex Technical Systems, Sandtorstrasse 1, 39106 Magdeburg, Germany

Received: June 10, 2008; Revised Manuscript Received: September 8, 2008

The dynamics of glycolytic waves in a yeast extract have been investigated in an open spatial reactor. At low protein contents in the extract, we find a transition from inwardly moving target patterns at the beginning of the experiment to outwardly moving spiral- or circular-shaped waves at later stages. These two phases are separated by a transition phase of more complex spatiotemporal dynamics. We have analyzed the pattern dynamics in these three intervals at different spatial scales by means of a Karhunen−Loève (KL) decomposition. During the initial phase of the experiment, the observed patterns are sufficiently described by the two dominant KL modes independently of the spatial scale. However, during the last stage of the experiment, at least 6 KL modes are needed to account for the observed patterns at spatial scales larger than 3 mm, while for smaller scales, 2 KL modes are still sufficient. This indicates that in the course of the experiment, the local glycolytic oscillators become desynchronized at spatial scales larger than 3 mm. Possible reasons for the desynchronization of the glycolytic waves are discussed.

1. Introduction

Synchronization phenomena have been investigated in many different systems of chemical, physical, or biological origin.[1−5] Besides the purely temporal description, spatiotemporal synchronization processes associated with dynamic pattern formation have recently gained increasing scientific interest, since in biological systems spatiotemporal (de)synchronization processes have important functional meanings. For example, traveling circular excitation waves on the heart muscle mediate its regular pacing and are indispensable for the survival of the organism. Here, desynchronization represents a pathologic event which may occur as the result of spiral break up of the circular waves, leading to heart failure.[6,7] Just the opposite functional meaning is realized in the brain, where localized synchronization of brain activity is a pathologic event that leads to malfunction in certain regions of the brain with subsequent disorders like Parkinson's resting tremor or epilepsy.[8,9] In the latter case, desynchronization via deep brain stimulation has been proven to be a promising therapeutic treatment.[10] These examples demonstrate that understanding the principles of (de)synchronization processes is a fundamental task in biomedicine and biotechnology.

Several experimental and theoretical studies on possible control mechanisms for synchronization have been performed, mainly on the basis of chemical or physical systems. For example, it was found that external white noise can lead either to synchronization or desynchronization of self-sustained oscillators, depending on the noise intensity and on the system properties.[11] For spatially extended systems, dynamics of higher complexity can be expected, also leading to more complex synchronization phenomena. On the basis of theoretical investigations of the FitzHugh−Nagumo model, the occurrence of noise-enhanced phase synchronization was predicted for excitable media.[12] Kheowan et al.[13] investigated an oscillatory variant of the Belousov−Zhabotinsky (BZ) reaction and found wave-mediated synchronization of coupled oscillatory cells with randomly distributed frequencies. Here, the competition between different pacemakers finally leads to a synchronized state, which is characterized by propagating phase−diffusion waves with constant phase difference. Global as well as local delayed feedback has been shown to be a powerful tool for synchronization/desynchronization of spatiotemporal patterns in chemical or physical systems.[14−16] Here, the feedback gain and the delay time are important parameters for controlling the synchronization strength.

Much less is known about the mechanisms that control synchronization in biological systems, although their functional meaning is evident. Glycolytic oscillations in yeast cells have been extensively investigated as a biological model system for an oscillatory medium, both theoretically[17,18] and experimentally.[19,20] Synchronization of glycolytic oscillations in individual cells within a dense cell population is mediated by acetaldehyde, an intermediate of alcoholic fermentation that is secreted by the cells during glycolytic sugar degradation.[21] Studies performed in a well-controlled continuous-flow stirred tank reactor (CSTR) revealed that also the input substrate to the glycolytic pathway (glucose) can mediate the synchronization.[22] The generation of glycolytic oscillations depends on the cell density,[23] which can be explained by the reduced amplitude of the extracellular acetaldehyde oscillations due to a larger extracellular volume in diluted cell populations.[24] So far, all of these studies have been performed in stirred cell suspensions, and the synchronization of these temporal oscillations is now well understood. However, spatiotemporal patterns arise when there is a coupling of the glycolytic flux with diffusive transport,[25] leading to more complex processes of synchronization/desynchronization.[26,27]

† Part of the "Karl Freed Festschrift".

* To whom correspondence should be addressed. Phone: ++49(0)391 6110 481. Fax: ++49(0)391 6110 543. E-mail: rstraube@mpi-magdeburg.mpg.de.

‡ Otto-von-Guericke University.

§ Vienna University of Technology.

⊥ Max-Planck-Institute for Dynamics of Complex Technical Systems.

10.1021/jp805087m CCC: $40.75
Published on Web 10/23/2008

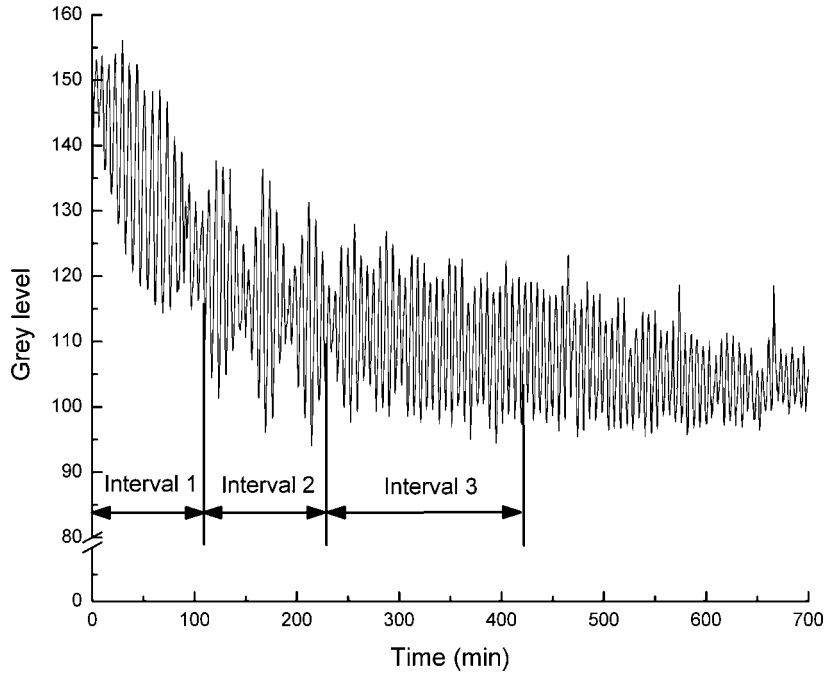

Figure 1. Local temporal oscillations of the NADH fluorescence intensity (~gray level) recorded over an area of 40 × 40 pixels^2. According to the observed dynamics, the experiment was divided into the three time intervals.

For example, traveling NADH and proton waves have been observed in yeast extract when oscillatory glycolysis is induced in the extract.[28] Moreover, intracellular traveling proton waves in neutrophil cells have been reported to result from oscillatory glycolysis in these cells.[29]

In the present paper, we investigate the dynamics of spatiotemporal pattern formation of glycolysis in a yeast extract at low protein content. In our experiments, we observe a transition from ordered inwardly propagating waves to more complex patterns. To elucidate the mechanisms leading to the transition from ordered to complex behavior and to identify the dominant spatial structures, we analyzed the dynamics of these spatiotemporal patterns by Karhunen−Loève (KL) decomposition. The KL decomposition, also known as proper orthogonal decomposition, is a well-established method which allows one to find a minimal linear representation for a given data set that is optimal in a certain statistical sense.[30] It has been successfully exploited to describe the catalytic CO oxidation on Pt surfaces[31] as well as the local characterization of spatiotemporal chaos in a reaction diffusion system.[32] When applied to spatiotemporal data $w(x, t)$, the KL decomposition yields a representation of the original signal in the form

$$w(x,t) = \sum_n A_n(t) Y_n(x)$$

where the space- and time-dependent parts are separated from each other. In particular, $Y_n(x)$ are orthonormal space-dependent basis functions, and $A_n(t)$ denote the corresponding orthogonal time-dependent amplitudes. The KL modes $Y_n(x)$ diagonalize the spatial two-point correlation function $C(x, x') = \langle w(x, t)w(x', t)\rangle$. The magnitude of the respective eigenvalues is a measure of the significance of the associated mode. In this sense, the eigenvalue spectrum can be used to separate the signal from the noise, leading to a systematic extraction of the relevant information. On the basis of the eigenvalue spectrum, one typically retains only the most dominant modes. In that case, the time-dependent amplitudes yield a low-dimensional representation of the original (high-dimensional) data set in a finite dimensional phase space. Interestingly, if the dynamics of the system under consideration is periodic in time or translationally invariant, the KL modes become simple Fourier modes.[30]

2. Methods Section

2.1. Experimental Methods. The experiments were performed with a cell-free yeast extract prepared from aerobically grown yeast *Saccharomyces carlsbergensis* (ATCC 9080). The methods for preparation of yeast extract have been described in detail in ref 33. The experiments were conducted in an open spatial reactor, which consisted of a 1.3 mm thick diffusive layer in contact with the content of a CSTR. The diffusive layer was composed of yeast extract that was immobilized in agarose gel. The protein content of the yeast extract was diluted with buffer (25 mM MOPS, 50 mM KCl, pH 6.5) such that its concentration in the gel was 24 mg/ml for all experiments. In the following, we will refer to this concentration as low because it is only half of the protein concentration of the undiluted yeast extract (≈50 mg/mL). The CSTR acts as a reservoir for the substrate and the necessary cofactors of glycolysis. A permanent supply of these substances to the CSTR was provided by a pump connected to stock solutions. Similarly, the gel layer (where all glycolytic enzymes are immobilized) was fed with substrates and cofactors from the CSTR by diffusion. Nonequilibrium conditions in the diffusive layer were achieved by exchange of substrates and products between the CSTR and the gel through the contact interface. Glycolytic waves have been monitored optically by means of NADH fluorescence since the glycolytic flux is coupled to the NAD^+/NADH oxidation/reduction cycle. The optical setup for in situ video- recording of the spatiotemporal processes is described elsewhere.[33] The measured video sequences were digitized at a rate of five images per minute. Each particular image was then rescaled from 540 × 740 to 80 × 100 pixel^2. One pixel corresponds to 1/46 mm.

2.2. Karhunen−Loève Analysis. To analyze our experiments, we apply the Karhunen−Loève (KL) method to a temporal sequence of two-dimensional video images. The experiments yield a set of $t = 1...n$ intensity (gray value) images $\{\tilde{B}^t\}$ of dimension

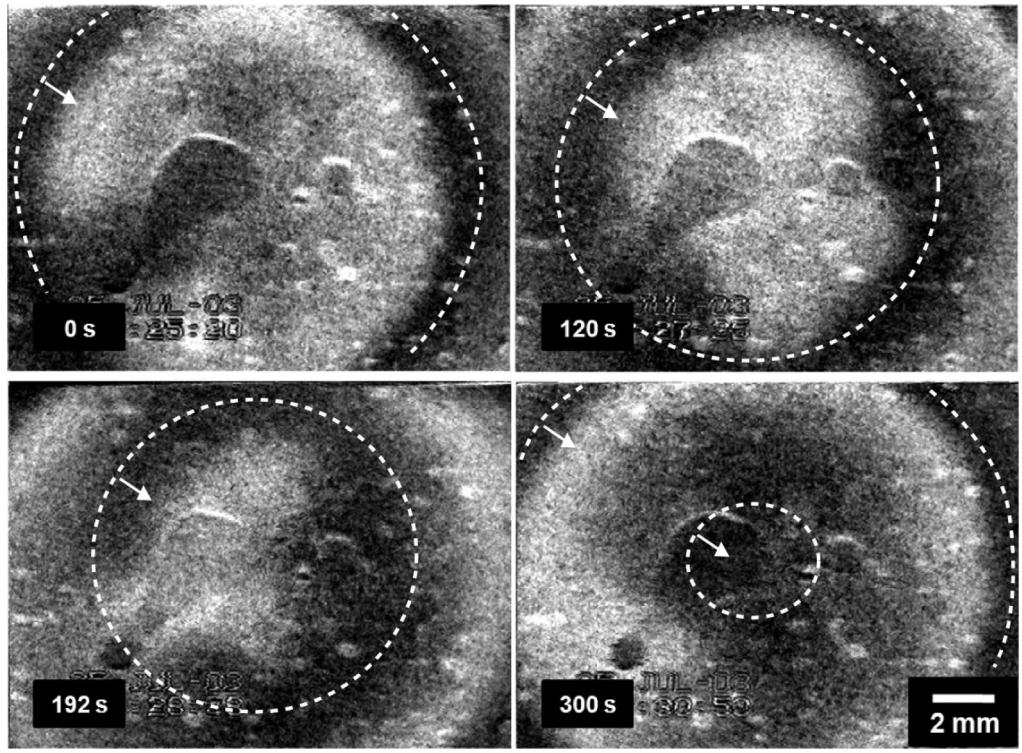

Figure 2. Inwardly propagating circular-shaped wave during the initial stage of the experiment (interval 1 in Figure 1). The shape of the circular wave is highlighted by white dashed lines, while the white arrows indicate the propagation direction (scale bar: 2 mm).

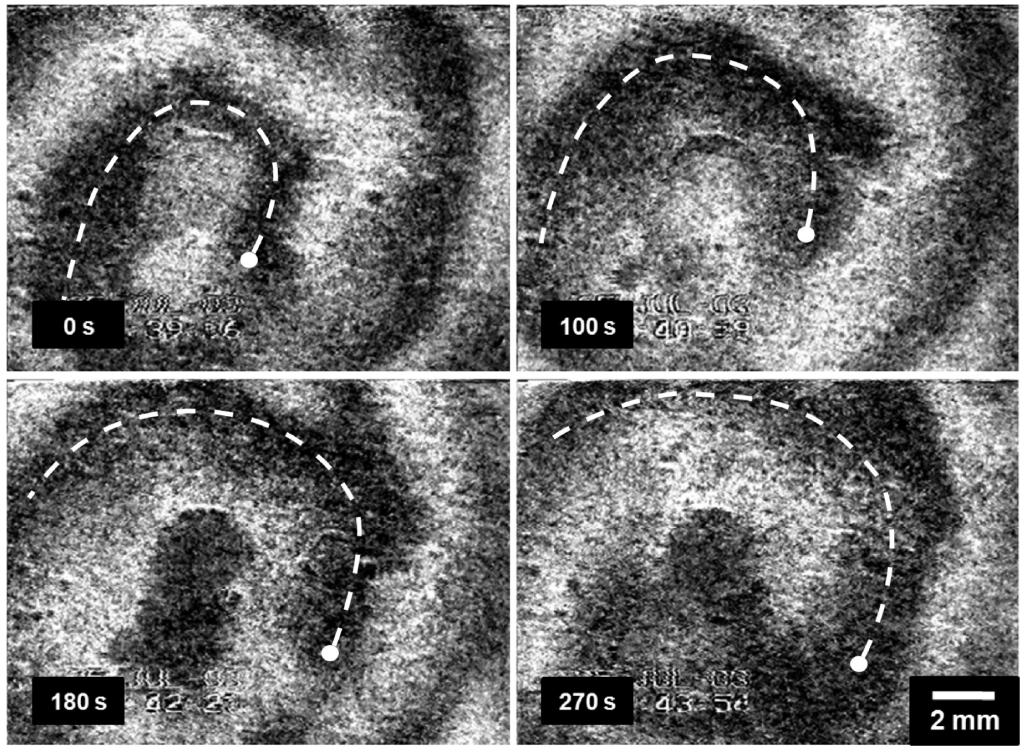

Figure 3. Outwardly propagating spiral wave during the last stage of the experiment (interval 3 in Figure 1). The shape of the spiral wave is highlighted by white dashed lines, while the white dot marks the spiral core (scale bar: 2 mm).

dim x·dim y. In this representation, a particular image $\tilde{B}^t$ is given by a matrix $\tilde{B}^t_{ij}$, where the (i, j)th entry denotes the gray value of the (i, j)th pixel in the image $\tilde{B}^t$. Next, the time average of the image sequence is subtracted from each measurement $B^t_{ij} = \tilde{B}^t_{ij} - (1/n)\sum_{k=1}^{n} \tilde{B}^k_{ij}$ such that the new data set $\{B^t\}$ has a vanishing mean value $\langle B^t \rangle = 0$. For explicit calculations, it is convenient to represent each intensity image by a vector instead of a matrix. This can be done by reordering the matrix elements in the row major form, that is, the rows of the image B^t are concatenated such that the matrix element B^t_{ij} is mapped to the vector component $b_{(i)q}$, where q is given by

$$q = j + (i - 1)\cdot \dim y \tag{1}$$

As a result, from the original set of n images, one large matrix of dimension $n \times (\dim x \cdot \dim y)$ is obtained. The corresponding matrix elements are of the form

$$b_{(t)q} = \begin{pmatrix} B_{ij}^1 & (1\text{st image}) \\ & \vdots \\ B_{ij}^n & (n\text{th image}) \end{pmatrix}$$

that is, each row, labeled by the index t, corresponds to one of the original (mean-value-centered) images B^t. The KL decomposition of the matrix $b_{(t)q}$ can be obtained from its singular value decomposition

$$b_{(t)q} = \sum_{r,s} u_{(t)r}\lambda_{rs}v_{sq} \quad \text{or} \quad b = u\lambda v^{\mathrm{T}} \tag{2}$$

as

$$b_{(t)q} = \sum_{l} a_l^t v_{lq} \quad \text{where} \quad a_l^t = \sum_{r} u_{(t)r}\lambda_{rl} \tag{3}$$

which yields the desired separation of the original data set into time-independent modes $v_{l(\cdot)}$ and their corresponding time-dependent amplitudes a_l^t. In eq 2, the superscript $(\cdot)^{\mathrm{T}}$ denotes matrix transposition whereas u and v are matrices whose columns are composed of left and right eigenvectors of b, respectively, while $\lambda_{rl} = \lambda_r\delta_{rl}$ denotes a diagonal matrix containing the associated singular values of b. The right eigenvectors v are also eigenvectors of the covariance matrix $C_{qr} = (n-1)^{-1}\sum_{t=1}^{n} b_{q(t)}b_{(t)r}$ or $C = (n-1)^{-1}b^{\mathrm{T}}b$, that is, we have

$$Cv = \Lambda v \quad \text{with} \quad \Lambda = \frac{\lambda^2}{n-1} \tag{4}$$

This relation defines the KL modes in eq 3, that is, they diagonalize the covariance matrix of the original data set. Note that each KL mode $v_{l(\cdot)}$ can be rearranged into a matrix m_{ij}^l with the help of eq 1. In terms of these matrices, the original image sequence $\tilde{B}_{ij}^t$ can be reconstructed from

$$\tilde{B}_{ij}^t = \frac{1}{n}\sum_{k=1}^{n}\tilde{B}_{ij}^k + \sum_{l} a_l^t m_{ij}^l \tag{5}$$

The eigenvalues Λ_l in eq 4 are all positive and can be ordered as $\Lambda_1 \geq \Lambda_2 \geq \ldots$. Their magnitude is a measure for the variance of the original data set projected along the lth KL mode since the coefficients a_l^t are, on average, uncorrelated, that is

$$\mathrm{var}(a) \equiv \frac{1}{n-1}\sum_{k} a_l^k a_m^k = \frac{\lambda_l^2}{n-1}\delta_{lm} = \Lambda_l\delta_{lm}$$

Experimental data sets usually exhibit some degree of redundancy due to correlations among certain variables. Accordingly, the eigenvalue spectrum will decay toward higher mode numbers. In this case, the original images $\tilde{B}_{ij}^t$ may well be reconstructed using only the first k modes in eq 5 (i.e., $l = 1, \ldots, k$). A widely used measure to determine the number of modes for reconstruction or representation of the original data set is the fraction of the statistical variance that is captured by the first k KL modes

$$V_k = \frac{\sum_{i=1}^{k}\Lambda_i}{\sum_{i=1}^{n}\Lambda_i} \qquad \frac{\Lambda_1}{\sum_{i=1}^{n}\Lambda_i} \leq V_k \leq 1 \tag{6}$$

For later reference, we also define the normalized eigenvalues σ_k as

$$\sigma_k = \frac{\Lambda_k}{\sum_{i=1}^{n}\Lambda_i} \tag{7}$$

3. Results

In all experiments with a low protein concentration in the yeast extract, we observed inwardly moving target patterns during the initial phase, while at a later stage, a transition to outwardly propagating waves takes place. However, these waves are not always of spiral shape but sometimes also appear as circular-shaped waves depending on intrinsic system parameters and/or initial conditions.

3.1. Transition from Inwardly Propagating Target Patterns to Outwardly Propagating Spirals. Figure 1 shows temporal oscillations of the NADH fluorescence averaged over a small area (40×40 pixel^2, taken from the total observation area of 540×740 pixel^2), which confirms that the glycolytic reaction system is in the oscillatory regime. The analysis of this time series in conjunction with the observed spatiotemporal patterns suggests a division of the experiment into three distinct time intervals. The first interval (0−120 min) is clearly transient and shows a net decrease of the NADH fluorescence. Here, an equilibration between the gel and the feeding solutions takes place since the metabolic/ionic compositions in the gel and those in the CSTR compartment are different at the start of the experiment. Interestingly, we observed large inwardly propagating circular waves (Figure 2) during this initial stage of the experiment (time interval 1). They have a wavelength and a wave velocity of 7 mm and 16 μm/s, respectively.

In the course of the second interval (120−240 min), a transition from inwardly propagating waves to outwardly propagating spiral waves was observed. The local dynamics acquires a second, incommensurate modulating frequency (Figure 1, interval 2). This quasi-periodic modulation could be caused by the competition between the inwardly propagating waves and the upcoming spiral waves, which, in general, will

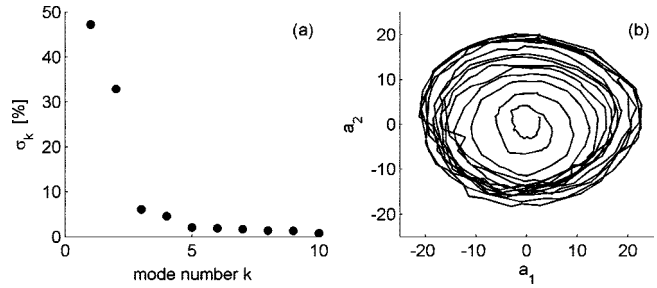

Figure 4. (a) Normalized eigenvalue spectrum σ_k for the KL analysis of the entire observation area in time interval 1; (b) phase portrait of the temporal amplitudes $a_1(t)$ and $a_2(t)$ associated with the first two KL modes for the same interval.

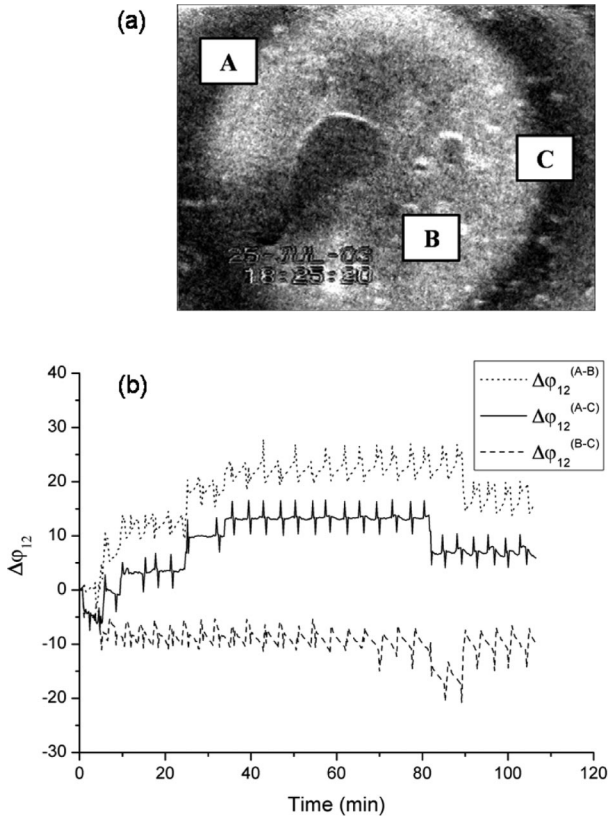

Figure 5. The white rectangles denoted as A, B, and C mark the regions over which a local KL analysis has been performed (a). Temporal behavior of the phase differences $\Delta\varphi_{12}^{(i-j)} = \varphi_{12}^{(i)} - \varphi_{12}^{(j)}$ during interval 1 with i, j = A, B, C and i ≠ j (b). The phases $\varphi_{12}^{(i)}$ between the first and second KL modes are calculated as $\Delta\varphi_{12}(t) = \arctan(a_2(t)/a_1(t))$, where the amplitudes $a_1(t)$ and $a_2(t)$ are obtained from a local KL analysis of the three different regions shown in (a).

select a different wavenumber with a correspondingly different oscillation frequency.

The last stage of the experiment (from 240 to 430 min) is characterized by outwardly propagating spiral waves (Figure 3) whose wavelength and wave velocity were determined as 5 mm and 10 μm/s, respectively.

3.2. KL Analysis of the Pattern's Coherence. The spatiotemporal dynamics in each time interval was separately analyzed by Karhunen−Loève decomposition. The KL eigenvalue spectrum for time interval 1 (Figure 4a) shows that 80% of the total variance is captured by the first two modes (V_2 = 0.80, cf. eq 6). Consequently, the inwardly propagating waves observed during the initial stage of the experiment are sufficiently described by the first two modes. Note that the obviously different variances for the first two KL modes are a direct consequence of the transient nature of the dynamics during time interval 1. The presence of two dominant modes reflects a high degree of spatial correlation of the spatiotemporal structures. Figure 4b shows the phase portrait of the temporal amplitudes $a_1(t)$ and $a_2(t)$ associated with the first two KL modes. The trajectory obviously approaches a limit cycle in the course of time, indicating that the spatiotemporal structures also evolve coherently in time.

To confirm that the glycolytic oscillations are truly synchronized in different regions of the gel reactor, we compared the phase differences between local oscillations in three different parts of the total area of observation. For this purpose, a local KL analysis was performed on the regions shown in Figure 5a. After about 20 min, the phase differences $\Delta\varphi_{12}$ between the first two KL modes assume a nearly constant value, indicating that the waves are synchronized and propagate uniformly with constant phase shift during time interval 1 (Figure 5b).

In time interval 2, where the transition from inwardly moving target patterns to outwardly moving spiral waves takes place, the number of leading KL modes increases (Figure 6a). To account for the same statistical variance as that during interval 1, at least six KL modes (V_6 = 0.86) are needed to describe the dynamical behavior of the waves. The first two KL modes are still dominant, capturing 46% of the total variance. The phase plane plot of the first two KL amplitudes reveals a more complex structure than the simple limit cycle behavior during interval 1. In accordance with the presence of two frequencies during

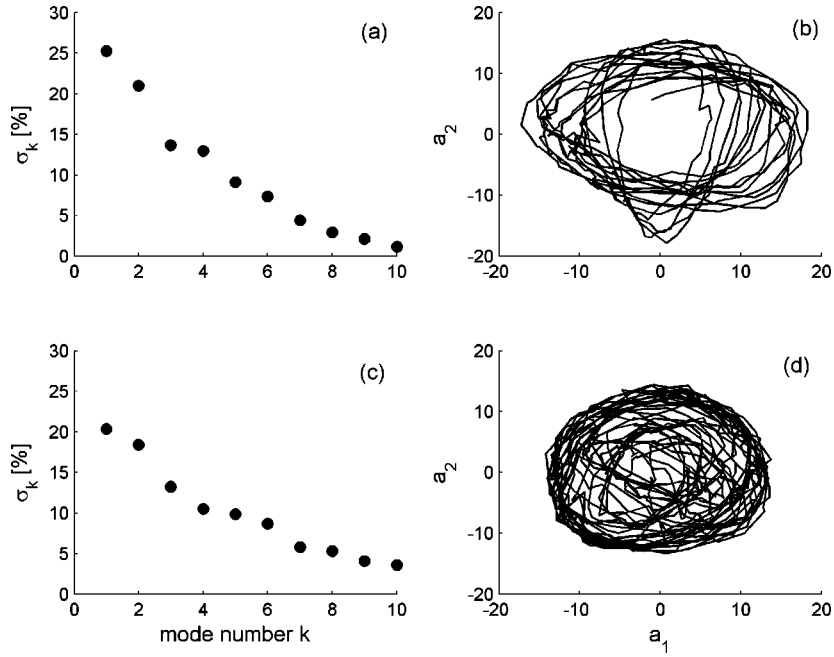

Figure 6. Normalized eigenvalue spectrum σ_k for the KL analysis of the entire observation area in time intervals 2 (a) and 3 (c). Phase portraits of the temporal amplitudes $a_1(t)$ and $a_2(t)$ associated with the first two KL modes for time intervals 2 (b) and 3 (d).

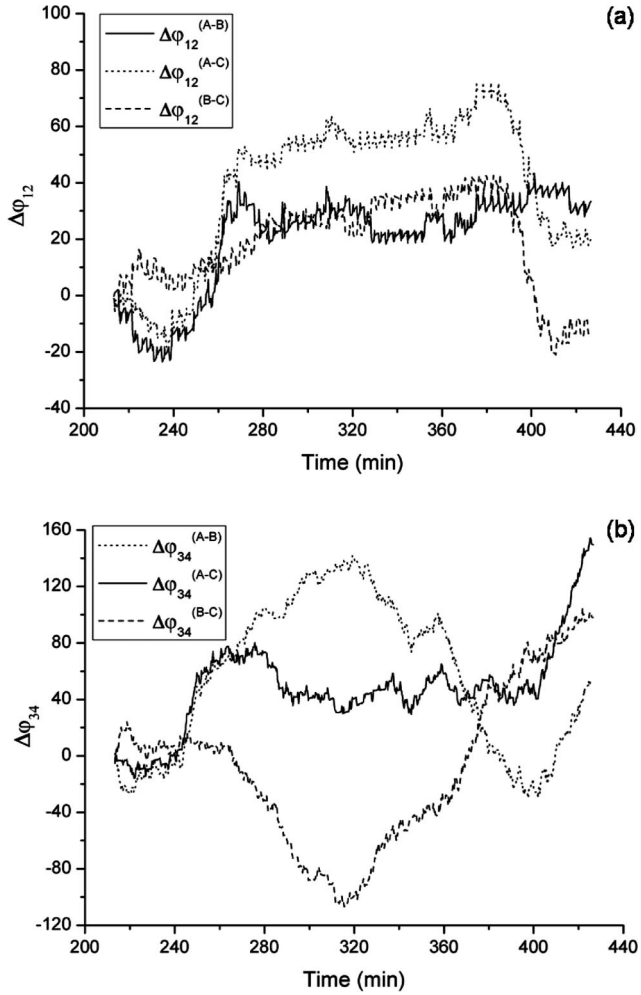

Figure 7. Temporal behavior of the phase differences during time interval 3 between (a) the first and second KL modes ($\Delta\varphi_{12}$) and (b) between the third and fourth KL modes ($\Delta\varphi_{34}$) obtained from a local KL analysis of the three different regions shown in Figure 5a.

interval 2 (cf. Figure 1), the trajectory in Figure 6b resembles a 2D projection of a higher dimensional torus.

The last stage of the experiment (interval 3) is characterized by outwardly propagating spiral waves. Similarly to the previous interval, at least six modes ($V_6 = 0.81$) are needed to reconstruct the dynamics of the spirals (Figure 6c). Interestingly, while the eigenvalue spectrum is comparable to that of interval 2, the phase plane projection of the first two KL amplitudes looks quite irregular (Figure 6d). Thus, the temporal behavior of the large-scale spatial structures observed during interval 3 (as measured by the dominant KL modes) is not coherent, despite the fact that coherently rotating spirals are visible during that period. This suggests that the transition to the irregular behavior during the later stages of the experiment is associated with some kind of spatial desynchronization, that is, that spatiotemporal coherence is retained only on smaller spatial scales. To corroborate this hypothesis, we again performed a local KL analysis of the three different regions shown in Figure 5a. The phase differences between the first two KL modes assume a nearly constant value during the time interval from 260 to 400 min (Figure 7a), while the average total variance captured by the first two KL modes is 86% ($V_2 = 0.86$). This indicates that the irregular structures appearing in the later stage of the experiment still retain some coherent behavior which is described by the first two KL modes. In contrast, the phase differences between the third and fourth KL modes show irregular behavior in time, pointing to spatial

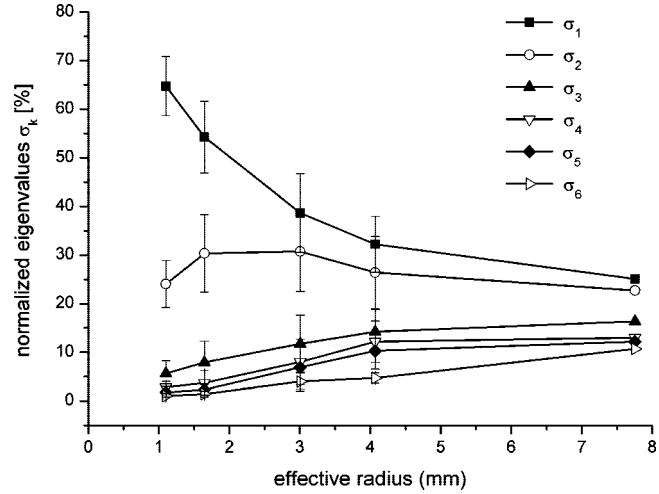

Figure 8. Eigenvalue spectrum as a function of the effective radius $r = (AO/\pi)^{1/2}$, where AO is the area of observation for which a local KL analysis was performed.

desynchronization (Figure 7 b) since the higher KL modes describe the spatial fine structure of the patterns.

3.3. Separation of Spatial Scales. The observation that the dynamics of the large-scale structure becomes highly irregular during interval 3 (Figure 6d) prompted us to investigate whether the spatiotemporal structures retain some coherence on smaller spatial scales. We found that in the last stage of the experiment, a separation of spatial scales takes place. On the large scale (the whole area of observation), the patterns are spatially desynchronized, as measured by the phase differences associated with the dominant KL modes which are obtained from a local KL analysis in different regions of the gel (Figure 7). However, on smaller scales, the patterns are still synchronized, as will be shown in the following.

First, we analyzed the dependence of the number of KL modes needed for a faithful representation of the spatiotemporal dynamics on the size of the area of observation (Figure 8). For this purpose, an effective radius was assigned to the local area of observation AO as $r = (AO/\pi)^{1/2}$. Then, a local KL analysis was performed for at least three different nonoverlapping regions of equal size that were arbitrarily chosen from the total area of observation. By making the area smaller and smaller, the average contribution of the first six KL modes to the spatiotemporal pattern during interval 3 was obtained as a function of the local observation area or, equivalently, as a function of the effective radius. Most importantly, the contribution of the first mode increased rapidly with decreasing radius. It captured 65% of the total variance for the smallest analyzed radius (1 mm). This is more than twice the contribution of the first mode (25%) when the entire image is analyzed by KL decomposition. The contribution of the higher modes is marginal for small radii and increases moderately for larger ones. Thus, the spatiotemporal patterns occurring during interval 3 are sufficiently described by the first two KL modes on spatial scales of $r \leq 3$ mm, where the mode spectrum exhibits a sharp transition (Figure 9e). In addition, the phase plane projection of the first two KL amplitudes exhibits simple limit cycle behavior, similar to that observed during interval 1 on the large scale (cf. Figure 4b), which demonstrates that they are evolving coherently in time.

Figure 9 summarizes the local coherence properties of the spatiotemporal patterns during all three intervals close to the transition point $r = 3$ mm. For intervals 1 and 3, the first two KL modes are sufficient to account for the locally observed patterns since there is a clear cutoff in the eigenvalue spectra

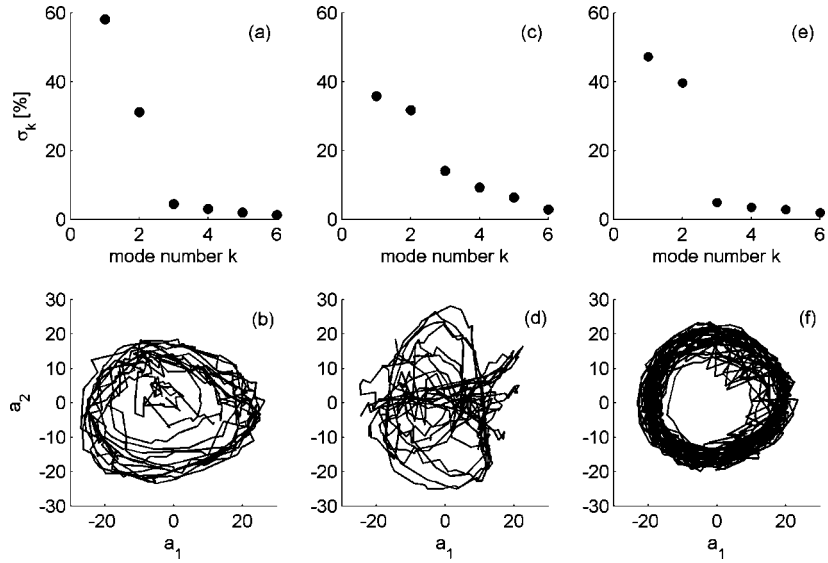

Figure 9. Comparison of the eigenvalue spectra and the phase portraits of the temporal amplitudes $a_1(t)$ and $a_2(t)$ associated with the first two KL modes for intervals 1 (a,d), 2 (b,e), and 3 (c,f). A local KL analysis was performed on a small observation area with an effective radius of 3 mm.

between the second and the higher modes (Figure 9a,e). Also, the corresponding phase space projections show a limit cycle behavior for the trajectories described by the corresponding KL amplitudes $a_1(t)$ and $a_2(t)$ (Figure 9b,f), which clearly demonstrates the local coherence of the spatiotemporal patterns. In contrast, the cutoff in the eigenvalue spectrum during interval 2 (Figure 9c) is less obvious, so that two KL modes are probably not sufficient to account for the local spatiotemporal dynamics during that interval. Moreover, the trajectory in the phase plane projection of the first two KL modes is highly irregular (Figure 9d), suggesting that the dominant modes are not evolving coherently in time during interval 2.

4. Discussion

The emerging spatiotemporal structures during glycolysis in yeast extracts in an open spatial reactor were investigated. Minutes after the initiation of the experiment, we observed inwardly moving target patterns. After 100 min, these patterns become unstable, and outwardly propagating spirals randomly emerge and vanish again shortly after they have been created. This transition region lasts for ~120 min until the propagation of the spirals is stabilized and the target patterns have disappeared during the third stage of the experiment (220−420 min).

Our results demonstrate that the transition from inwardly moving target waves to outwardly moving spiral waves is accompanied by desynchronization and spatial decoherence. In particular, the inwardly moving target waves observed during interval 1 (Figure 1) are coherent in space and time, both globally (total area of observation) and locally, since in both cases they are described by only two KL modes (spatial coherence; see Figures 4a, 9a) and the phase plane projection of the associated KL amplitudes yields a simple limit cycle behavior (temporal coherence; see Figures 4b, 9b). By contrast, the spatiotemporal patterns observed during interval 2 are neither spatially nor temporally coherent, which holds locally (down to spatial scales of 1 mm) and globally. Interestingly, the spiral dynamics observed during the last stage of the experiment is characterized by two different spatial scales. On scales of $r > 3$ mm (where r corresponds to the effective radius of the observation area), more than two KL modes are needed to account for the dynamics of the observed patterns. In addition, the phase plane projection of the first two KL amplitudes is highly irregular. By contrast, on scales of $r \leq 3$ mm, two KL modes seem to be sufficient to describe the observed spatiotemporal dynamics, and the phase plane projection exhibits a simple limit cycle behavior (Figure 9a,b). Note that the wavelength of the observed spirals is ~5 mm, which is slightly smaller than the diameter (6 mm) of the largest area where spatiotemporal coherence is still observed. This suggests that the spirals observed during interval 3 are desynchronized on large scales while each isolated spiral still represents a (locally) coherent spatiotemporal structure.

Similar results have been obtained with a model of cAMP signaling for aggregation patterns of the slime mold *Dictyostelium discoideum*.[34] During the developmental path, a transition between concentric waves to spiral waves occurred as the result of local desynchronization of the cells at larger scales. This behavior was explained as due to changes of enzyme activities.[34] Interestingly, in this model, cell clusters of small size still exhibited synchronized behavior, while at larger scales, desynchronization led to the formation of spirals.

The inwardly propagating target patterns have only been encountered during the initial phase of the experiment. Similarly to inwardly propagating spiral waves (see ref 36), these spatiotemporal structures have so far rarely been observed in real experiments, while theoretical studies of the complex Ginzburg−Landau equation suggest that they should generically occur in oscillatory media close to the onset of oscillations.[37−39] According to these investigations, inwardly propagating target and spiral waves are generic solutions of the complex Ginzburg−Landau equation with a negative phase velocity such that the phase velocity and the group velocity point in opposite directions.

On the other hand, it is possible that spatial gradients in certain system parameters may also lead to inwardly propagating waves. Since the formation of such gradients during the initial preparation of yeast extracts in the gel cannot be excluded, we must consider this scenario as an alternative explanation for the occurrence of inwardly propagating target waves. As we have already pointed out, in the beginning of the experiment, the metabolic/ionic compositions in the gel and those in the reactor are not balanced. A quasi-stationary fluorescence level

of NADH is reached only at the end of interval 2 (Figure 1). Thus, possible initial gradients may be degraded in the course of the experiment, while the metabolic/ionic compositions in the gel and those in the reactor settle into a stationary state, causing the spontaneous, since not externally controllable, transition from inwardly propagating waves to outwardly propagating spiral waves. Interestingly, it has been reported for the Belousov−Zhabotinsky reaction that chemical gradients can lead to spatial desynchronization of three-dimensional scroll waves.[40]

Alternatively, the spatial coupling within the oscillatory reaction medium may change and eventually cause the desynchronization. Kheowan et al.[13] have shown that a strong spatial coupling in an oscillatory BZ medium with randomly distributed frequencies leads to the generation of synchronized phase waves, whereas a weak spatial coupling favors spatial desynchronization. Accordingly, in the glycolytic system, a decrease in the spatial coupling may also cause the transition from inwardly propagating circular waves (synchronized state) to outwardly propagating spiral waves (desynchronized state). Such changes in the spatial coupling may arise due to diffusive instabilities.

A possible application of our results may be related to the electrical excitation of the heart. Here, the generation of spiral waves induces spatial desynchronization that finally leads to cardiac death. One possibility for the termination of this chaotic behavior is multisite pacing.[35] If the desynchronization is space dependent, as we have shown for glycolytic waves, the knowledge of the effective radius, as determined here by Karhunen−Loève analysis, may provide an estimate for the optimal size of the pacing electrodes.

5. Conclusion

We have investigated the spatiotemporal dynamics of glycolysis in an open spatial reactor filled with a yeast extract that was fixed in a gel matrix. At low protein concentration in the extract, a spontaneous transition from inwardly moving circular-shaped waves to outwardly moving spiral waves was observed. A systematic Karhunen−Loève analysis of the corresponding spatiotemporal patterns showed that this transition is associated with desynchronization of the local glycolytic oscillators at spatial scales larger than 3 mm. A similar behavior has been observed during the developmental path of the slime mold *Dictyostelium discoideum*,[34] which suggests that spiral-mediated desynchronization might be a general communication mode in biological systems.

Acknowledgment. We thank Lutz Brusch and Ernesto M. Nicola for helpful discussions and the Deutsche Forschungsgemeinschaft (DFG) for financial support.

References and Notes

(1) Bub, G.; Shrier, A.; Glass, L. *Phys. Rev. Lett.* **2005**, *94*, 028105.
(2) Kiss, I. Z.; Rusin, C. G.; Kori, H.; Hudson, J. L. *Science* **2007**, *316*, 1886–1889.
(3) Pikovsky, A.; Rosenblum, M.; Kurths, J. *Synchronization. A Universal Concept in Nonlinear Sciences*; Cambridge University Press: Cambridge, U.K., 2001.
(4) Manrubia, S. C.; Mikhailov, A. S.; Zanette, D. H. *Emergence of Dynamical Order: Synchronization Phenomena in Complex Systems*; World Scientific: Singapore, 2004.
(5) Hauser, M. J. B.; Schneider, F. W. *J. Chem. Phys.* **1994**, *100*, 1058–1065.
(6) Zipes, D. P.; Jalife, J. *Cardiac Electrophysiology. From Cell to Bedside*; Saunders Company: Philadelphia, PA, 1995.
(7) Tusscher, K. H. W. J. T.; Hren, R.; Panfilov, A. V. *Circ. Res.* **2007**, *100*, e87–e101.
(8) Lenz, F. A.; Kwan, H. C.; Martin, R. L.; Tasker, R. R.; Dostrovsky, J. O.; Lenz, Y. E. *Brain* **1994**, *117*, 531–543.
(9) Volkmann, J.; Joliot, M.; Mogilner, A.; Ioannides, A. A.; Lado, F.; Fazzini, E.; Ribary, U.; Llinas, R. *Neurology* **1996**, *46*, 1359–1370.
(10) Tass, P. A. *Biol. Cyb.* **2002**, *87*, 102–115.
(11) Goldobin, D. S.; Pikovsky, A. *Phys. Rev. E* **2005**, *71*, 045201R.
(12) Neiman, A.; Schimansky-Geier, L.; Cornell-Bell, A.; Moss, F. *Phys. Rev. Lett.* **1999**, *83*, 4896–4899.
(13) Kheowan, O.-U.; Mihaliuk, E.; Blasius, B.; Sendina-Nadal, I.; Showalter, K. *Phys. Rev. Lett.* **2007**, *98*, 074101).
(14) Tokuda, H.; Zykov, V. S.; Ohta, T. *Phys. Rev. E* **2007**, *75*, 066203.
(15) Vanag, V. K.; Yang, L.; Dolnik, M.; Zhabotinsky, A. M.; Epstein, I. R. *Nature* **2000**, *406*, 389–391.
(16) Schöll E. *Nonlinear Spatio-Temporal Dynamics and Chaos in Semiconductors*; Cambridge University Press: Cambridge, U.K., 2001.
(17) Madsen, M. F.; Danø, S.; Sørensen, P. G. *FEBS J.* **2005**, *272*, 2648–2660.
(18) Wolf, J.; Passarge, J.; Somsen, O. J. G.; Snoep, J. L.; Heinrich, R.; Westerhoff, H. V. *Biophys. J.* **2000**, *78*, 1145–1153.
(19) Richard, P.; Teusink, B.; Westerhoff, H. V.; Van Dam, K. *FEBS Lett.* **1993**, *318*, 80–82.
(20) Gosh, A.; Chance, B. *Biochem. Biophys. Res. Commun.* **1964**, *16*, 174–181.
(21) Richard, P.; Bakker, B. M.; Teusink, B.; Van Dam, K.; Westerhoff, H. V. *Eur. J. Biochem.* **1996**, *235*, 238–241.
(22) Danø, S.; Sørensen, P. G.; Hynne, F. *Nature* **1999**, *402*, 320–322.
(23) Poulsen, A. K.; Petersen, M. Ø.; Olsen, L. F. *Biophys. Chem.* **2007**, *125*, 275–280.
(24) Danø, S.; Madsen, M. F.; Sørensen, P. G. *Proc. Natl. Acad. Sci. U.S.A.* **2007**, *104*, 12732–12736.
(25) Goldbeter, A. *Proc. Natl. Acad. Sci. U.S.A.* **1973**, *70*, 3255–3259.
(26) Zhang, L.; Gao, Q.; Wang, Q.; Zhang, X. *Biophys. Chem.* **2007**, *125*, 112–116.
(27) Battogtokh, D.; Tyson, J. J. *Phys. Rev. E* **2004**, *70*, 026212.
(28) Mair, T.; Müller, S. C. *J. Biol. Chem.* **1996**, *271*, 627–630.
(29) Petty, H. R.; Worth, R. G.; Kindzelskii, A. L. *Phys. Rev. Lett.* **2000**, *84*, 2754–2757.
(30) Holmes, P.; Lumley, J.; Berkooz, G. *Turbulence, Coherent Structures, Dynamical Systems and Symmetry*; Cambridge University Press: Cambridge, U.K., 1996.
(31) Suchorski, Yu.; Beben, J.; Imbihl, R. *Surf. Sci.* **2000**, *454−456*, 331–336.
(32) Meixner, M.; Zoldi, S. M.; Bose, S.; Schöll, E. *Phys. Rev. E* **2000**, *61*, 1382–1385.
(33) Bagyan, S.; Mair, T.; Dulos, E.; Boissonade, J.; DeKepper, P.; Müller, S. C. *Biophys. Chem.* **2005**, *116*, 67–76.
(34) Lauzeral, J.; Halloy, J.; Goldbeter, A. *Proc. Natl. Acad. Sci. U.S.A.* **1997**, *94*, 9153–9158.
(35) Pumir, A.; Nikolski, V.; Hörning, M.; Isomura, A.; Agladze, K.; Yoshikawa, K.; Gilmour, R.; Bodenschatz, E.; Krinsky, V. *Phys. Rev. Lett.* **2007**, *99*, 208101.
(36) Vanag, V. K.; Epstein, I. R. *Science* **2001**, *294*, 835–837.
(37) Nicola, E. M.; Brusch, L.; Bär, M. *J. Phys. Chem. B* **2004**, *108*, 14733–14740.
(38) Gong, Y.; Christini, D. J. *Phys. Rev. Lett.* **2003**, *90*, 088302.
(39) Aranson, I. S.; Kramer, L. *Rev. Mod. Phys.* **2002**, *74*, 99–143.
(40) Storb, U.; Neto, C. R.; Bär, M.; Müller, S. C. *Phys. Chem. Chem. Phys.* **2003**, *5*, 2344–2353.

JP805087M